Desalination and Water Treatment
www.deswater.com
doi: 10.5004/dwt.2018.22646

127 (2018) 231–242
September

Facile synthesis of ethylenediamine-modified magnetic chitosan composite and its adsorption property

Min Wu, Yunshan Bai*, Kewang Wang, Wenyun Li, Dandan Xu, Hongzhu Ma*

Key Laboratory of Applied Surface and Colloid Chemistry, Ministry of Education, School of Chemistry and Chemical Engineering, Shaanxi Normal University, Xi'An, Shaanxi 710119, People's Republic of China, Tel. +86 29 81530726; Fax: +86 29 81530727; emails: hzmachem@snnu.edu.cn (H. Ma), baiys@snnu.edu.cn (Y. Bai), 2447617131@qq.com (M. Wu), 350385605@qq.com (K. Wang), 605142289@qq.com (W. Li), 992004343@qq.com (D. Xu)

Received 8 November 2017; Accepted 19 June 2018

ABSTRACT

In this study, ethylenediamine-modified magnetic chitosan composite (MCS-NH_2) adsorbent was synthesized facilely by one-pot method. The structural analysis of the composite were obtained from Fourier-transform infrared, X-ray powder diffraction, thermogravimetric analysis, vibrating sample magnetometer, scanning electron microscopy, field transmission electron microscopy, zeta potential, Brunauer–Emmett–Teller specific surface areas, and pore structure. Its adsorption capacities toward anionic dye Orange II (ORII) were studied in a batch system. The highest ORII removal of 94.3% was obtained at the optimum conditions: pH 7.07, initial ORII concentration 100 mg L^{-1}, adsorbent dose 3 g L^{-1}, and room temperature (293 K) at 30 min. In addition, the effect of various salts on the adsorption performance of MCS-NH_2 was also investigated. The kinetic adsorption isotherms and thermodynamics were also studied and the experimental data fitted better with the pseudo-second-order kinetic and the Freundlich model, with spontaneous and exothermic characteristics. The results showed that MCS-NH_2 composite exhibited excellent adsorption capacities toward anionic dye, which should have potential applications in effluent treatment in printing and dyeing industry.

Keywords: Ethylenediamine; Magnetic; Chitosan; ORII; Adsorption

1. Introduction

The textile industry effluents contain large amounts of colorants that are most difficult to biodegrade. Several methods, such as chemical precipitation, ion exchange, reverse osmosis, oxidation/reduction, adsorption, filtration, coagulation, electrolysis, evaporation, electroplating, activated sludge, aerobic and anaerobic treatment, have been used to remove the pollutants with high removal efficiencies [1–5]. In terms of initial cost, flexibility and simplicity of design, ease of operation, and insensitivity to toxic pollutants, adsorption is superior to other techniques.

Nowadays, the adsorption of contaminants from wastewater by nanomaterials has drawn enormous interest. Among various nanoadsorbents that have been applied for dye adsorption, magnetic nanoparticles (MNPs) have attracted great attention because of their distinctive properties such as low toxicity, large surface area, easy surface modification, and separation under an external magnetic field [6–9]. However, because of the anisotropic dipolar attraction effect, naked MNPs usually easily aggregated in aqueous solutions, thus reducing its sorption capacity and restricting its extensive use [10].

In order to improve their stability, Fe_3O_4 NPs are often modified with functionalized materials or biopolymers before applications. Chitosan (β-(1–4)-linked-d-glucosamine) is famous for functionality, biocompatibility, nontoxicity, adsorption property, low price, and eco-friendly [11,12]. It contains a substantial number of amino and hydroxyl groups, which can bind pollutants and interact with Fe_3O_4 to

* Corresponding author.

form a good dispersion of the NPs [13], which is benefit and widely used for dyes and heavy metals removal [14–17].

In this study, a simple one-pot synthesis approach was adopted to prepare ethylenediamine-modified magnetic chitosan nanocomposite (MCS-NH_2). Its adsorption property toward anionic dye Orange II (ORII), and the effect of the operating parameters, such as the dosage of the adsorbent, contact time, temperature, the initial concentration of ORII, the initial pH, various inorganic salts on ORII removal, and the reusability of MCS-NH_2, were investigated systematically. The kinetic, adsorption isotherms and thermodynamics were also studied to further elucidate the adsorption behavior and the possible mechanism was also proposed.

2. Materials and method

2.1. Materials

Chitosan $(C_6H_{11}NO_4)_n$ with molecular weight 5 × 10^4 (>90% degree of deacetylation) was derived from China (Golden-Shell Biochemical Co., Ltd.). Ethylenediamine ($NH_2CH_2CH_2NH_2$, purity 99%), epichlorohydrin (C_3H_5ClO), cetyl trimethyl ammonium bromide ($C_{19}H_{42}NBr$), sodium dodecyl sulfate ($C_{12}H_{25}SO_4Na$), ferric chloride hexahydrate ($FeCl_3{\cdot}6H_2O$), ferrous sulfate ($FeSO_4{\cdot}7H_2O$), acetic acid (CH_3COOH), ammonium hydroxide($NH_3{\cdot}H_2O$), sodium chloride (NaCl), calcium chloride ($CaCl_2$), sodium sulfate (Na_2SO_4), and ORII ($C_{16}H_{11}N_2O_4SNa{\cdot}5H_2O$, A.R.) in analytically pure were obtained from Sinopharm Chemical Reagent Co., Ltd. , Xi'An, China, and used without further purification.

2.2. Preparation of MCS-NH_2

The adsorbent was obtained through one-step method: Fe_3O_4 particles were prepared by coprecipitating Fe^{2+} and Fe^{3+} ions by $NH_3{\cdot}H_2O$ solution in the presence of MCS-NH_2 based on previous method [18–20]. Typically, Ferric chloride hexahydrate (2.17 g) and ferrous sulfate (0.77 g) were dissolved in 50 mL deionized water at a concentration of 0.2 M iron ions to obtain the magnetic fluid. Chitosan solution was prepared by dissolving 0.35 g chitosan in 100 mL of 1% (v/v) acetic acid with stirring for 2 h until completely dissolved. And then the magnetic fluid was added to the solution slowly. Chemical precipitation was achieved at 298 K under vigorous stirring by addition of $NH_3{\cdot}H_2O$ solution until the solution turning black (pH 10). After that the solution stirred for another 1 h to form coated chitosan layer, chitosan on the surface of the MNPs is available for further modification to obtain more active sites. Then, 10 mL epichlorohydrin was added with stirring for 2 h at 333 K and 15 mL ethylenediamine was introduced excessively to get the maximum amino incorporated according to Ref. [20]. The reaction mixture was stirred for 3 h at 333 K, then the solid products were separated using an external magnet and washed with distilled water followed by ethanol for three times and finally dried in a vacuum oven at 333 K to obtain MCS-NH_2. The synthesis of MCS-NH_2 is given in Fig. 1.

2.3. Adsorption and desorption experiments

In this study, the adsorption performance of MCS-NH_2 was investigated by adding 0.03 g MCS-NH_2 into 10 mL ORII dye solution (50, 100, 150, or 200 mg L^{-1}) in a 50 mL glass flask at various temperatures (298, 303, 313, or 323 K) under an agitation speed of 200 rpm. After a certain time, the adsorbent was separated using external magnet as shown in Fig. 1. The concentration of ORII was then determined by measuring the absorbance of the solution at 484 nm (λ_{max} for ORII), using a UV–vis spectrophotometer (UVT6, Beijing Purkinje General Instrument Co. Ltd, China). The color removal (R) of ORII and adsorption amount (q_t) were calculated according to Eqs. (1) and (2) as follows:

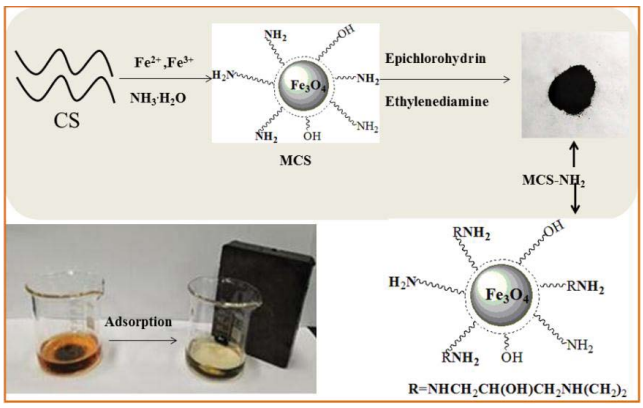

Fig. 1. Synthesis and adsorption properties of MCS-NH_2.

$$R\% = \frac{(C_0 - C_t)}{C_0} \times 100\% \quad (1)$$

$$q_t = \frac{(C_0 - C_t)V}{W} \quad (2)$$

where C_0 and C_t (mg L^{-1}) are the respective ORII concentration in solution at initial time and at time t (min); q_t (mg g^{-1}) is the amount of ORII adsorbed onto MCS-NH_2 at time t; V (mL) is the volume of ORII solution; and W (mg) is the mass of MCS-NH_2.

For desorption and recycle studies, 0.03 g MCS-NH_2 loaded with ORII was desorbed using 10 mL ethanol, at 298 K and contact time of 2 h. The adsorbent after desorption dried in a vacuum oven at 333 K and was reused in the next adsorption experiment. The color removal (R) of ORII and adsorption amount (q_t) were also calculated according to Eqs. (1) and (2).

Effect of various salts: The effect of various salts (NaCl, $CaCl_2$, and Na_2SO_4 in 10 g L^{-1}) or NaCl with various concentrations on the adsorption performance was investigated. After 30 min, the adsorbent was separated using external magnet and the concentration of ORII was then determined according to the previous procedure.

2.4. Characterization of the adsorbents

The crystallization and morphologies of the adsorbents were analyzed by X-ray powder diffraction (XRD, Rigaku, Japan). Fourier-transform infrared (FTIR) spectra were taken on a Tensor 27 (Bruker, Germany) instrument in the range of 4,000–400 cm^{-1}. The Brunauer–Emmett–Teller (BET) specific surface areas and pore structure were obtained from nitrogen adsorption–desorption data at 373 K using a BET (ASAP2020

Mike, USA). Scanning electron microscopy (SEM, Quanta 200, FEI) and field transmission electron microscopy (TEM, Tecnai G2 F20, FEI) were used to confirm the surface morphology and dispersion of adsorbent. Thermogravimetric analysis (TGA) measurements were carried out on a thermoanalyzer systems (TA, USA), with a temperature range of 25°C–800°C at a heating rate of 10°C min^{-1}. The magnetic properties of the samples were studied at room temperature using a vibrating sample magnetometer (VSM, Lakeshore 735, USA) by sweeping the magnetic field from −10,000 to +10,000 Oe. Zeta potentials of the samples were determined using a micro-electrophoresis meter (ZEN3690, Malvern). A certain amount of the adsorbents was dispersed in distilled water with various pH values before this measurement.

3. Results and discussion

3.1. Characterization of the adsorbents

The FTIR spectra of Fe_3O_4 (a), CS (b), MCS (c), MCS-NH_2 (d), and MCS-NH_2-ORII (e) are shown in Fig. 2. For the Fe_3O_4, the band at 585 cm^{-1} was attributed to Fe-O group, the band around 3,419 cm^{-1} was related to the –OH group of adsorbed water [21].

For the CS (b), the band at 3,442 cm^{-1} was attributed to the stretching vibration band of –NH_2 and –OH. The characteristic peak of CS at 2,874 cm^{-1} was attributed to the stretching vibration of –CH and –CH_2 [20]. The stretching vibration of N–H band was observed at 1,654 cm^{-1} [22]. The band at 1,380 cm^{-1} could be assigned to the deformation vibration of CH_3 [1]. The band at 1,084 cm^{-1} indicated the combined effect of C–N stretching vibration of primary amines and the C–O stretching vibration from the primary alcohol in chitosan [23].

All of the characteristic peaks of CS were observed in MCS (Fig. 2(c)). The band at around 585 cm^{-1} was assigned to Fe–O bond vibration, which indicated the presence of Fe_3O_4

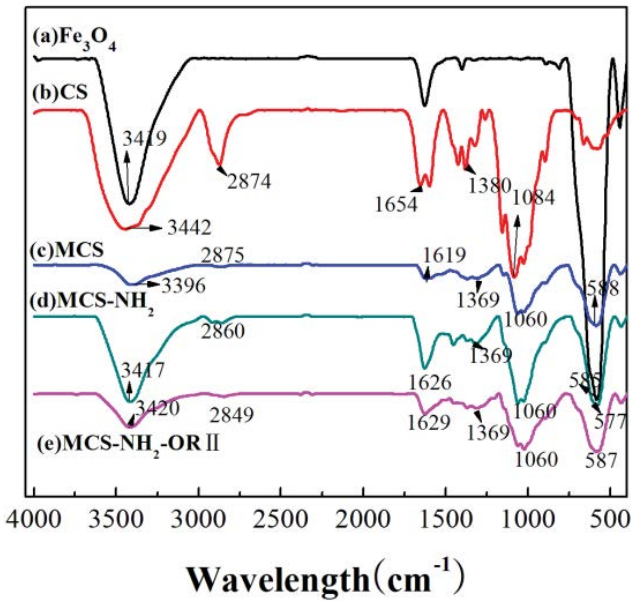

Fig. 2. FTIR spectra of Fe_3O_4 (a), CS (b), MCS (c), MCS-NH_2 (d), and MCS-NH_2-ORII(e).

as a result of the successful coating procedure. The main reason of Fe_3O_4 coated by chitosan was that the surface of iron oxide with negative charges has an affinity toward chitosan, thus protonated chitosan could coat the magnetite particles by the electrostatic interaction [24].

The intensity of the peak at 3,396 cm^{-1} attributed to the stretching vibration of the N–H bond with O–H strengthened and the peak shifted to 3,417 cm^{-1} for MCS-NH_2 (Fig. 2(d)). The peaks of N–H bending vibration and C–N stretching vibration of MCS-NH_2 observed at 1,626 and 1,080 cm^{-1}, respectively, were stronger than those of MCS, probably due to that more NH_2 attached to MCS.

After ORII adsorption (Fig. 2(e)), the band of overlapping of –NH and –OH stretching vibration shifted to 3,420 cm^{-1}, indicating that –OH joined in ORII adsorption [20]. A decrease in intensity of the N–H bending vibration at 1,629 cm^{-1} was also observed. These results indicated that hydroxyl and amino groups both involved in ORII adsorption [25].

Fig. 3(a) shows XRD patterns of Fe_3O_4, CS, and MCS-NH_2. Five characteristic peaks marked by their indices (220), (311), (400), (511), and (440) were observed for Fe_3O_4, which were consistent with the database in JCPDS file (PDF No. 65-3107) and revealed the spinel structure of resultant Fe_3O_4 nanoparticles [26,27]. The CS exhibited a typical diffraction peak at 2θ of around 20°, which was attributed to intermolecular hydrogen bond between amino and hydroxyl groups [28] and revealed its amorphous nature [29]. Quite weak diffraction lines of MCS-NH_2 composite indicated Fe_3O_4 nanoparticles have been coated by amorphous chitosan [21,30].

TGA measurement provides evidence to prove the reduction of organic matter. TGA curve of Fe_3O_4 showed weight loss about 3.2% below 150°C, which was due to the water physically adsorbed on the Fe_3O_4 surface as shown in Fig. 3(b) [11]. At 250°C–350°C, the weight losses of 15.74% and 18.95% for MCS and MCS-NH_2 respectively, were mainly assigned to the degradation and deacetylation of functional groups of chitosan [31]. The weight loss of MCS-NH_2 was more than MCS, indicating ethylenediamine has been incorporated in the composite. The final temperature of decomposition was approximately 750°C. About 51.32% and 47.82% of Fe_3O_4 in the MCS and MCS-NH_2 samples were determined.

The pH of zero point charge (pH_{zpc}) and zeta potential of MCS and MCS-NH_2 at different pHs are shown in Fig. 3(c). The pH_{zpc} values of 7.46 and 8.17 were observed for MCS and MCS-NH_2, respectively, indicating that more cationic amino group has been introduced during the aminated process. Negative zeta potentials above pH_{zpc} and positive values below pH_{zpc} were exhibited for MCS and MCS-NH_2, indicating the pH-response properties of the adsorbents. More positive zeta potentials of MCS-NH_2 were detected than that of MCS, suggesting that more –NH_2 have been incorporated.

The magnetic properties of samples were researched at room temperature and VSM curves are shown in Fig. 3(d). The values of saturation magnetization (M_s) of MCS and MCS-NH_2 were determined to be 33.12 and 29.41 emu g^{-1}, respectively, lower than that of the pure Fe_3O_4 (53.08 emu g^{-1}), maybe due to the nonmagnetic chitosan layer decreasing the relative content of the Fe_3O_4 in the sample and the

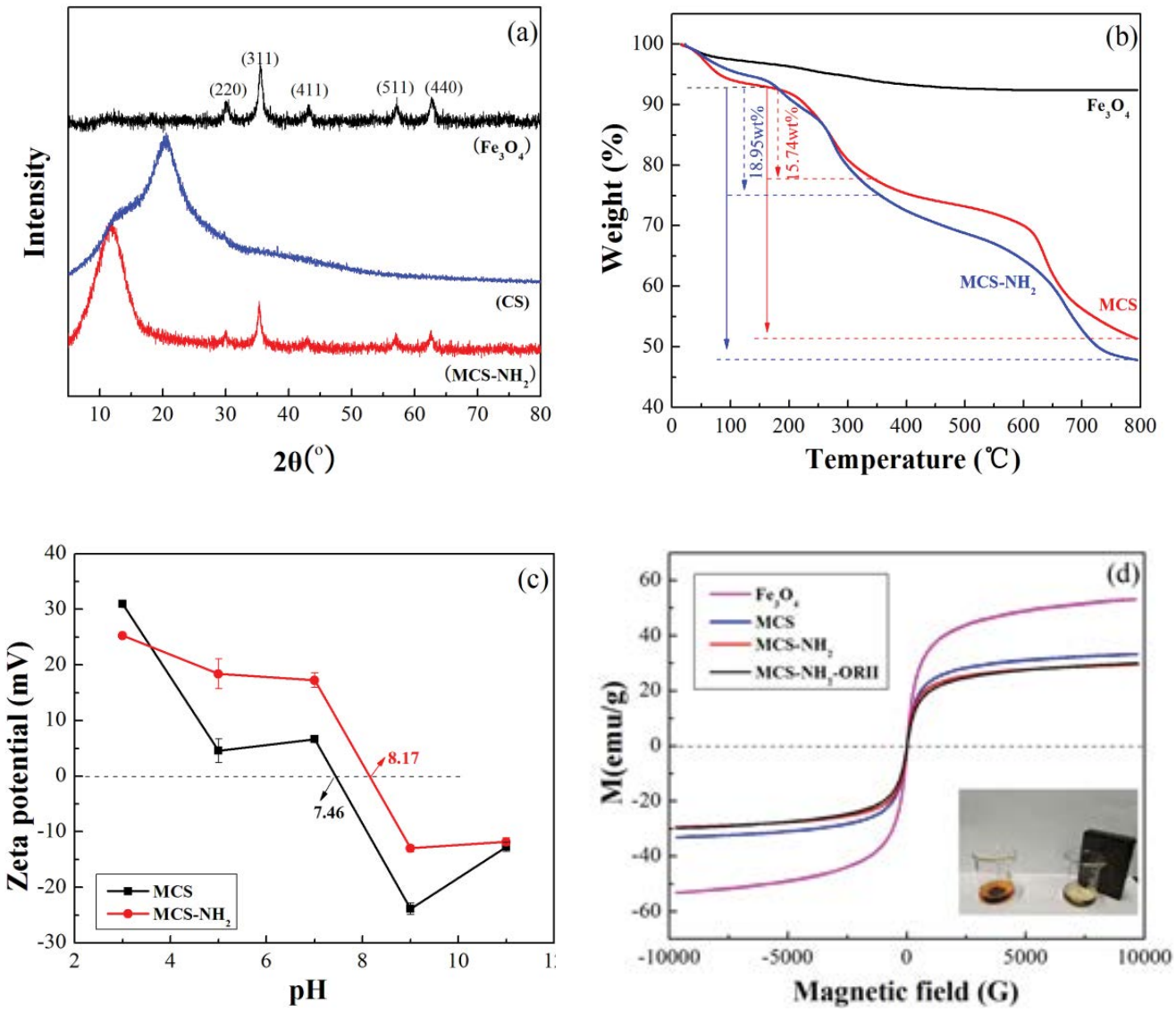

Fig. 3. XRD patterns (a), TGA curves (b), zeta potential (c), and VSM curves (d) of various adsorbents.

shielding effect on the naked Fe_3O_4 surface [19,32]. There was no hysteresis loss (Hc = 0 Oe) observed, indicating that the samples were superparamagnetic in nature. Moreover, the excellent magnetic responses of the prepared nanoparticles were also demonstrated by the easy separation of the sorbents from solution by an external magnet (inset in Fig. 3(d)), which is important for collection, regeneration, and reutilization of the sorbents. Similar values of saturation magnetization of MCS-NH_2 (29.41 emu g^{-1}) and MCS-NH_2-ORII (29.79 emu g^{-1}) were observed, suggesting the magnetic strength of MCS-NH_2 was almost kept constant during the reuse experiments.

The SEM and TEM analyses were performed to confirm the surface characteristics of the adsorbents (Fig. 4). Fe_3O_4 exhibited improved randomly dispersed particles in MCS-NH_2 [9], and the chitosan layer was distributed and coated around Fe_3O_4 particles [21, 23]. The chitosan coating process was affected weakly the agglomeration, maybe due to this it has occurred only on the surface of particle, which was consistent with reference reported [19].

The specific surface area and pore size distribution of the MCS-NH_2 and Fe_3O_4 were determined by the (BET method and relevant parameters are listed in Table 1. Specific surface area is an intrinsic property of any porous and powered particle which can divulge crucial information about its adsorption properties [33]. The BET surface area, pore size, and total pore volume for Fe_3O_4 were 103.41 m^2 g^{-1}, 14.06 nm, and 0.36 cm^3 g^{-1}, respectively, higher than those of MCS-NH_2. As is well-known, larger surface area is superior to smaller one for providing higher adsorption capacity [33], indicating that higher removal of ORII could not merely be owing to larger surface area.

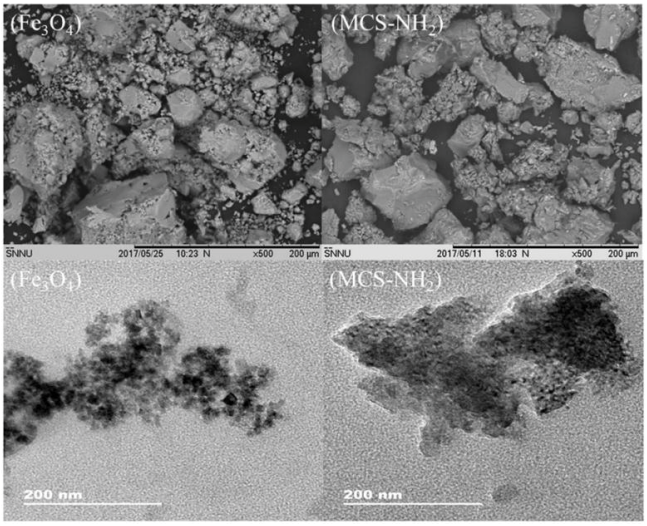

Fig. 4. SEM and TEM images of Fe_3O_4 and MCS-NH_2.

Table 1
Porosity parameters of Fe_3O_4, MCS and MCS-NH_2

Adsorbents	BET surface area (m^2 g^{-1})	Average pore size (nm)	Total pore volume (cm^3 g^{-1})
Fe_3O_4	103.41	14.06	0.36
MCS	26.72	5.90	0.04
MCS-NH_2	2.87	3.97	<0.01

3.2. Optimization of adsorption parameters

3.2.1. The adsorption capacities of various adsorbents

Fig. 5(a) shows the adsorption capacities of various adsorbents toward ORII under the same conditions. As can be seen, the adsorption amounts of 16.12, 24.00, and 33.94 mg g^{-1} were obtained for Fe_3O_4, MCS, and MCS-NH_2, respectively, indicating that chitosan coating and aminated modification improved the performance of the adsorbent. Considering the highest adsorption amount for ORII, MCS-NH_2 was selected in the further study.

3.2.2. The effect of contact time and adsorbent dose

The effect of contact time on removal percentage (Fig. 5(b)) demonstrated that the adsorption for ORII onto MCS-NH_2 was rapid. Clearly, the adsorption capacity sharply increased within the first 20 min and no significant changes were observed in the next 30 min. Excellent color removal of 94.3% was attained in 30 min. Furthermore, the color removal of ORII increased from 62.1% to 95.87% with increasing MCS-NH_2 dose from 0.5 to 9 g L^{-1} (inset in Fig. 5(b)). The fast ORII removal rate at the beginning might be attributed to the large numbers of available active sites on the surface of MCS-NH_2. After that, the adsorption became slower owing to the increased number of occupied adsorption sites and the slower diffusion of ORII into the inner hole of the composite [34,35]. All the adsorption equilibrium was achieved within 60 min. It was reported that a long time was needed to attain equilibrium for dyes with several adsorbents, such as chitosan/organoclay bionanocomposites [36], chitosan cross-linked with ethylenediamine composites [37], and other adsorbents [38,39]. In contrast, in this study, rapid adsorption of ORII onto MCS-NH_2 was achieved, which should have potential application in treatment of real industry wastewater.

3.2.3. The effect of temperature

The removal and adsorption amount decreased with the temperature increasing (Fig. 5(c)), indicated that the adsorption was an exothermic reaction. What's more, the increasing temperature likely influenced the intermolecular hydrogen bond between amino and hydroxyl groups and the internal structure of the adsorbents [20]. So the adsorption of ORII onto MCS-NH_2 in the further experiment was studied at room temperature (298 K).

3.2.4. The effect of the initial concentration of ORII

The adsorption amount of MCS-NH_2 increased from 15.66 to 72.10 mg g^{-1} with the concentration of ORII varied from 50 to 250 mg L^{-1} at pH 7.07 (Fig. 5(d)). This mainly might be attributed to the increase in concentration gradient in the system, which resulted in the enhanced efficiency of ORII adsorption [40,41]. Hence a higher initial concentration of dye enhanced the sorption process.

3.2.5. The effect of the initial pH

It can be observed that the highest removal percentage was obtained at pH 7 (Fig. 5(e)), which can be attributed to the impacts of pH on the surface function groups of adsorbent, surface charge, formation of ion species, and the interactions between functional adsorbent and ORII molecules [26]. Based on zeta potential analysis, in aqueous solution below pH 7.0, the protonated dye molecules formed due to the large amount of hydrogen ions might compete with NH_3^+, leading to the decrease in the anionic dye species interaction with the cationic active sites [42,43]. On the other hand, at the lower pH conditions, the dissociations of functional groups (like carboxyl, amino, and hydroxyl) were difficult [20]. When the solution pH increased from 7 to 11, the removal percentage decreased from 94% to 60%. This phenomenon can be explained that more OH^- in the alkaline solution competed with the anionic ORII molecules to be adsorbed on the surface of the MCS-NH_2 while OH^- predominated [44].

3.2.6. Recycle of MCS-NH_2

In this study, the reusability of MCS-NH_2 was investigated by a consecutive adsorption–desorption process. The regenerated adsorbents were used in the adsorption–desorption cycle for three times, and the results are illustrated in Fig. 5(f). The dye removal decreased from 94.3% to 88.71%, which might be due to the blockage of some active sites and the changes in the chemistry and the structure of the adsorbent [45].

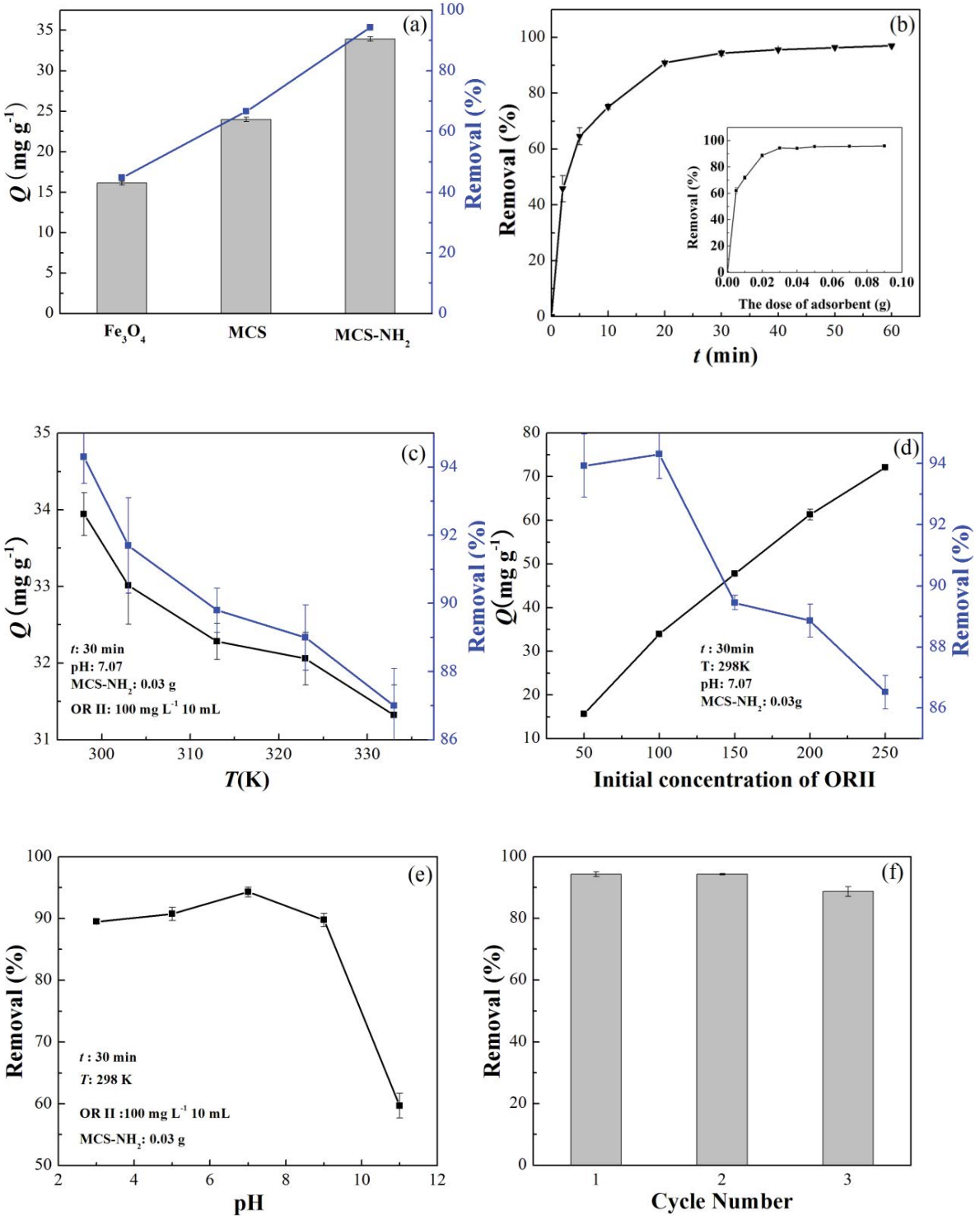

Fig. 5. Effect of parameters on ORII removal or adsorption capacity (a–e) and recycle of MCS-NH_2 (f).

3.2.7. The effect of type and concentration of coexisted salts

Dye-laden wastewaters released from textile industries contain various types of salts, with the concentration of 10–25 g L^{-1}, which may screen the electrostatic interaction of opposite charges in adsorbents and the dye molecules, and decrease the amount of dye adsorbed [46–48]. Here, the effect of inorganic salts, NaCl, $CaCl_2$, and Na_2SO_4, with the concentration of 0–20 g L^{-1} on removal of ORII was studied (Figs. 6(a) and 6(b)). A detrimental effect was observed for various inorganic salts (NaCl, $CaCl_2$, and Na_2SO_4), and the removal decreased with increasing concentration of NaCl in

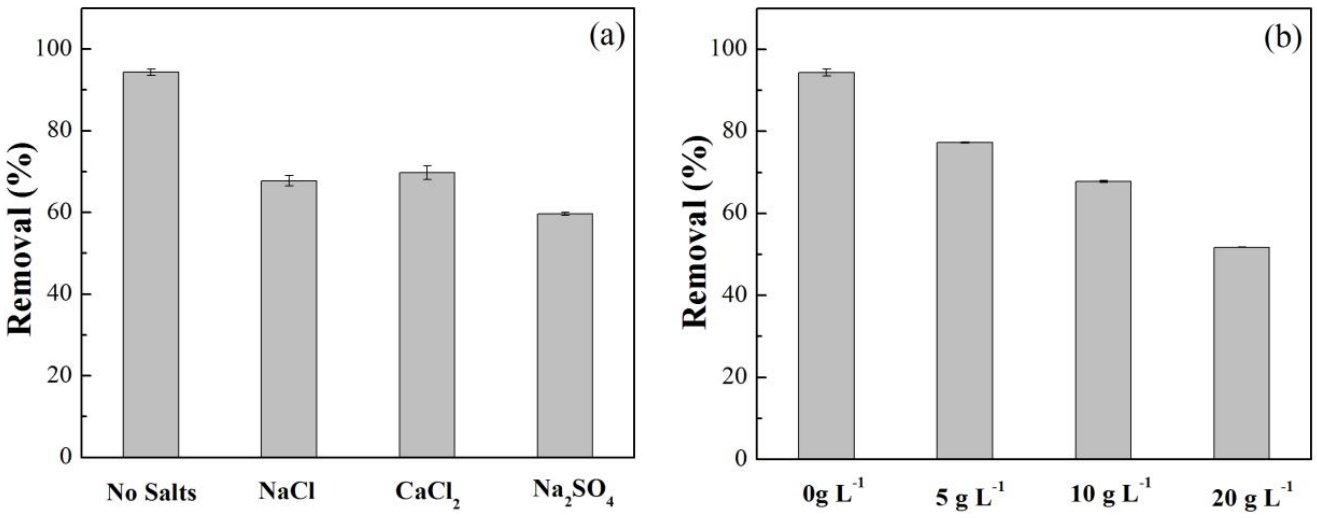

Fig. 6. Effect of type of inorganic salts (a) and concentrations of NaCl (b) on ORII removal (298 K; 100 mg L^{-1}; 10 mL; pH = 7.07; 3 g L^{-1} MCS-NH_2).

the experimental range. In the absence of NaCl, 94% of ORII was adsorbed after 30 min, while only 77.35%, 68.1%, and 51.7% of removal were observed with the concentration of NaCl increased from 5 to 20 g L^{-1}. The inhibition effect may be caused by the increasing ionic strength in the solutions leading to a suppression of the electrostatic interactions, which resulted the inhibition effect of the dyes adsorbed [47]. More information of the effect of inorganic salts would be studied in the further study.

3.3. Kinetic studies

The initial concentration provides an important driving force to overcome all mass transfer resistances and determine the rate of sorption, so the kinetic and thermodynamic studies of adsorption with different concentrations of dyes have been studied. The adsorption kinetics was investigated using three kinetic models, namely pseudo-first-order, pseudo-second-order, and Weber–Morris intraparticle diffusion model.

The pseudo-first-order equation can be expressed as follows:

$$\ln\left(q_e - q_t\right) = \ln q_e - k_1 t \tag{3}$$

The pseudo-second-order equation can be expressed as follows:

$$\frac{t}{q_t} = \frac{1}{k_2 q_e^2} + \frac{1}{q_e} t \tag{4}$$

where q_e and q_t (mg g^{-1}) are the amount of ORII adsorbed onto adsorbents at equilibrium and at time t, respectively. k_1 (min^{-1}) is the pseudo-first-order rate constant and k_2 (g mg^{-1} min^{-1}) is the pseudo-second-order rate constant.

Weber–Morris intraparticle diffusion model is the most common internal mass transfer model and is used to verify the resistance to mass transfer of the adsorbate for the adsorbent in the adsorption process [49].

The equation can be expressed as follows:

$$q_t = K_{id} t^{0.5} + C \tag{5}$$

where q_t (mg g^{-1}) is the amount of ORII adsorbed onto adsorbents at time t; K_{id} (mg g^{-1} $min^{-0.5}$) is the intraparticle diffusion constant; and C is the constant related to the boundary layer thickness.

The kinetic plots and parameters are listed in Fig. 7 and Tables 2 and 3. The correlation coefficient (R^2) of the pseudo-second-order model was higher than that of pseudo-first-order model. What's more, the experimental adsorption capacities $q_{e,exp}$ are close to the theoretical values of $q_{e,2}$, indicating that the adsorption of ORII onto MCS-NH_2 composite could be described well by the pseudo-second-order model, and the adsorption process was controlled by chemical adsorption. In addition, the pseudo-second-order rate constant (k_2) decreased with increasing initial ORII concentration, suggesting that the time required to reach adsorption equilibrium increased with increasing initial concentration [50].

Fig. 7(c) presents three separate regions with different slopes, indicating that the intraparticle diffusion was not the rate-limiting step for the whole adsorption process, that is, it was a multistep limited adsorption process.

The first sharper portion of the plot indicated that surface adsorption of the ORII dye was governed by a boundary layer effect. C is the constant related to the boundary layer thickness. The higher the value of C, the greater the effect of the boundary layer and the more dependent the adsorption process on the diffusion [49]. The second linear portion showed intraparticle diffusion. The third curved portion attributed to the attainment of equilibrium [41,51]. As shown in Fig. 7(c) the plots did not go through the origin, indicating the adsorption of ORII involved boundary and intraparticle diffusion.

3.4. Adsorption isotherm studies

Adsorption isotherm is used to describe the adsorbent capacity and its surface properties of adsorbent. Several models,

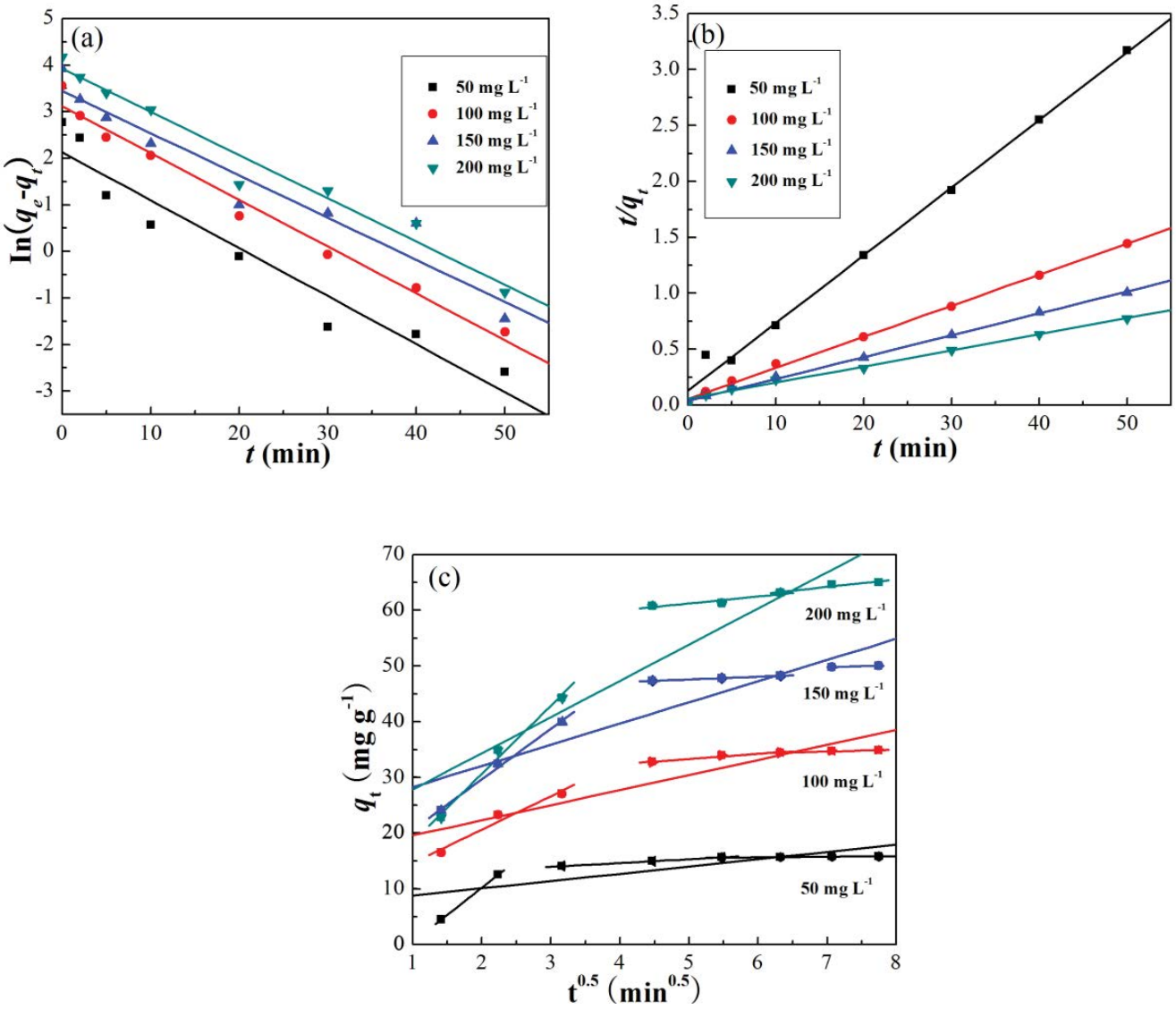

Fig. 7. The pseudo-first-order (a), pseudo-second-order (b), and intraparticle diffusion (c) kinetics plots for the adsorption of ORII onto MCS-NH_2 (298 K; 10 mL; pH = 7.07; 3 g L^{-1} MCS-NH_2).

Table 2
The kinetics parameters for the adsorption of ORII onto MCS-NH_2 (adsorbent: 3.0 g L^{-1}, contact time: 2–60 min, original pH 7.07, 298 K)

C_0 (mg L^{-1})	$q_{e,exp}$ (mg g^{-1})	Pseudo-first-order model			Pseudo-second-order model		
		$q_{e,1}$ (mg g^{-1})	k_1 (min^{-1})	R_1^2	$q_{e,2}$ (mg g^{-1})	k_2 (g mg^{-1} min^{-1})	R_2^2
50	15.85	8.3993	0.1029	0.9837	16.5316	0.0284	0.9936
100	34.88	22.5235	0.1004	0.9347	36.1011	0.0139	0.9974
150	50.05	31.2138	0.0905	0.9334	51.0725	0.0103	0.9975
200	65.00	50.6465	0.0929	0.9691	68.3995	0.0044	0.9923

such as Freundlich, Langmuir, Sips, Redlich–Peterson, and Toth, are widely used to correlate adsorption equilibrium [52]. In this study, Freundlich and Langmuir models were applied to describe the adsorption characteristic between adsorbent and ORII.

The Langmuir isotherm describes the equilibrium between the surface of solid and the solution as a reversible chemical equilibrium [53]. Langmuir model is based on the assumption such as: (1) monomolecular layer adsorption; (2) all adsorption sites are identical and energetically equivalent;

Table 3
The whole (a) and multisteps (b) intra-particle diffusion parameters of ORII onto MCS-NH_2 (adsorbent: 3.0 g L^{-1}, contact time: 2–60 min, original pH 7.07, 298 K)

(a)

C_0 (mg L^{-1})	C (mg g^{-1})	K_{id} (mg g^{-1} $min^{-0.5}$)	R^2
50	7.48	1.30	0.6016
100	16.86	2.71	0.8450
150	24.44	3.80	0.8388
200	21.34	6.49	0.8651

(b)

C_0 (mg L^{-1})	K_{id1}	C_1 (mg g^{-1})	R_1^2	K_{id2}	C_2 (mg g^{-1})	R_2^2	K_{id3}	C_3 (mg g^{-1})	R_3^2
50	9.79	9.35	1	0.68	11.92	0.9999	0.09	15.15	0.9442
100	6.01	8.62	0.9629	0.92	28.71	0.9622	0.32	32.40	0.9896
150	9.07	11.54	0.9957	0.48	45.17	0.9987	0.35	47.36	1
200	12.23	6.21	0.9883	1.26	54.92	0.8729	1.30	55.12	0.9253

(3) each site can accommodate only one molecule or atom; and (4) there is no interaction between adsorbents [20].

The Langmuir model can be represented as follows:

$$\frac{C_e}{q_e} = \frac{1}{K_L q_m} + \frac{C_e}{q_m} \tag{6}$$

where C_e (mg L^{-1}) is the equilibrium concentration of ORII solution; q_e (mg g^{-1}) is the amount of ORII adsorbed per unit weight of adsorbents at equilibrium; q_m (mg g^{-1}) is the maximum adsorption capacity; and K_L (L mg^{-1}) is the equilibrium constant of Langmuir equation related to the adsorption free energy.

$$R_L = \frac{1}{1 + K_L C_0} \tag{7}$$

The parameter R_L indicates the favorability of adsorption as follows: the value of R_L = 0 is irreversible adsorption; $0 < R_L < 1$ is favorable adsorption; R_L = 1 is linear adsorption; and $R_L > 1$ indicates unfavorable adsorption [45]. In this study, R_L calculated was in the range of 0–1 ($0 < R_L < 1$), so the adsorption of ORII was favorable adsorption and spontaneous.

Freundlich isotherm model is the earliest empirical equation based on the adsorption on reversible heterogeneous surfaces [52].

The equation is defined by the following equation:

$$\ln q_e = \ln K_F + \frac{1}{n} \ln C_e \tag{8}$$

where C_e is the equilibrium concentration of ORII solution (mg L^{-1}); q_e is the amount of ORII adsorbed per unit weight of adsorbents at equilibrium (mg g^{-1}); and K_F and n are the Freundlich constants related to the adsorption capacity and intensity.

The Langmuir and Freundlich isotherm fitting curves with the experimental data are shown in Fig. 8 and parameters are listed in Table 4. The correlation coefficient of the Freundlich model was much higher than that of Langmuir model, indicating the Freundlich model described the adsorption process better [54] and the adsorption capacity decreased with the temperature increasing, which was also consistent with the effect of temperature (Fig. 5(c)).

It is generally stated that the values of n gives the favorability of adsorption. When the value of n is higher than 1, it represents strong adsorption of ions onto the surface of adsorbent [53]. From Table 4, the exponent n values were higher than 1, representing the favorable adsorption condition in this adsorption process.

3.5. Thermodynamics

The thermodynamic parameters for the adsorption process can be used to deduce the adsorption mechanism. The standard Gibbs free energy change ΔG^0 (kJ mol^{-1}), standard enthalpy change ΔH^0 (kJ mol^{-1}), and standard entropy change ΔS^0 (J mol^{-1} K^{-1}) were calculated using the dependence of thermodynamic equilibrium constant (K_C) on temperature as follows (Eq. (12)):

$$\Delta G^0 = -RT \ln K_C \tag{9}$$

$$\Delta G^0 = \Delta H^0 - T\Delta S^0 \tag{10}$$

$$\ln K_C = -\frac{\Delta H^0}{RT} + \frac{\Delta S^0}{R} \tag{11}$$

where K_C can be calculated using Eq. (12) as follows:

$$K_C = \frac{C_A}{C_e} \tag{12}$$

where R (8.314 J mol^{-1} K^{-1}) is the ideal gas constant; C_A (mg L^{-1}) is the concentration of ORII adsorbed onto MCS-NH_2 at equilibrium; and C_e (mg L^{-1}) is the equilibrium concentration of ORII adsorbed.

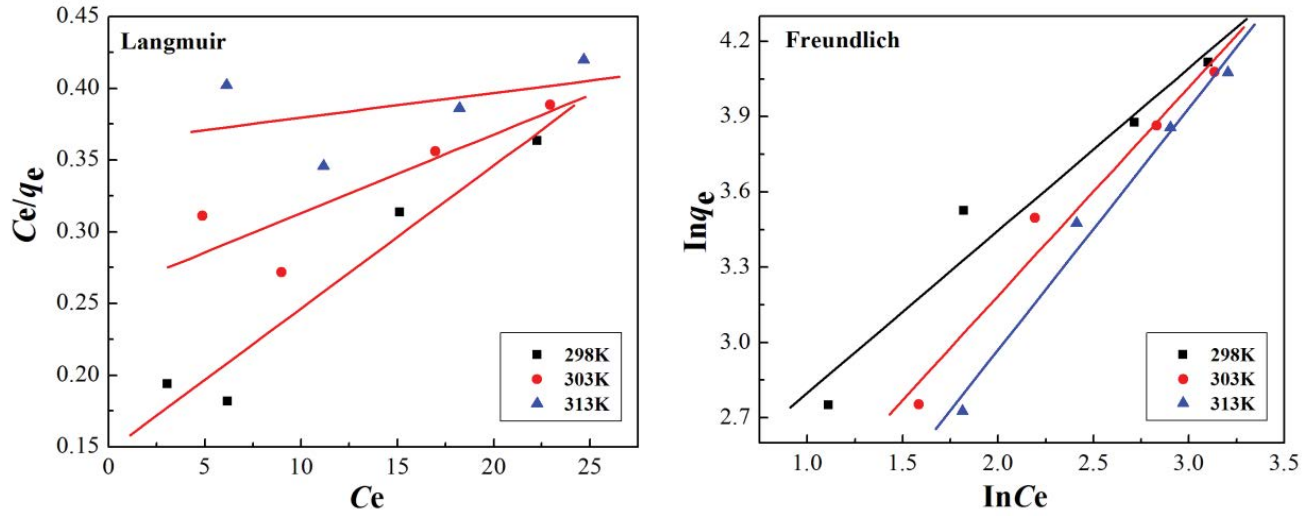

Fig. 8. The Langmuir and Freundlich models of ORII adsorption onto MCS-NH_2 (10 mL; pH = 7.07; 3 g L^{-1} adsorbent; contact time: 30 min).

Table 4
The adsorption isotherm parameters of ORII adsorption onto MCS-NH_2 (adsorbent: 3.0 g L^{-1}, contact time: 30 min, original pH 7.07, ORII: 50–200 mg L^{-1})

T (K)	Langmuir				Freundlich		
	q_m (mg g^{-1})	K_L (L mg^{-1})	R_L	R^2	K_F	n	R^2
298	100.50	0.0676	0.07042–0.2326	0.9473	8.6040	1.5459	0.9480
303	182.48	0.0212	0.1908–0.4854	0.7476	4.6007	1.2047	0.9677
313	581.40	0.0047	0.5155–0.8097	0.1949	2.8345	1.0374	0.9816

ΔH^0 and ΔS^0 were obtained from the slope and intercept of ln K_C versus $1/T$ as shown in Fig. 9 and the calculated values of the thermodynamic parameters are listed in Table 5. The negative values of ΔH^0, ΔS^0, and ΔG^0 indicated the exothermic, decreased randomness, and spontaneous nature of adsorption process. The absolute value of the ΔG^0

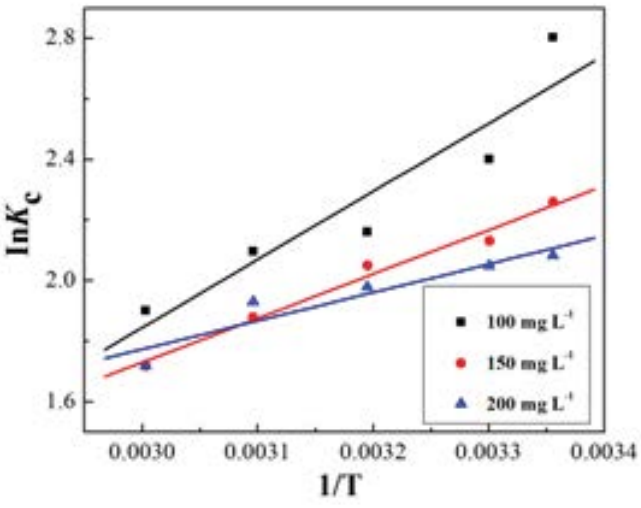

Fig. 9. Plot of ln K_C versus $1/T$ for adsorption of ORII on MCS-NH_2.

Table 5
Thermodynamic parameters for the adsorption of ORII onto MCS-NH_2 (adsorbent: 3.0 g L^{-1}, contact time: 30 min, original pH 7.07)

C (mg L^{-1})	T (K)	ΔG^0 (kJ mol^{-1})	ΔH^0 (kJ mol^{-1})	ΔS^0 (J mol^{-1} K^{-1})
100	298	−6.55	−18.70	−40.76
	303	−6.35		
	313	−5.94		
	323	−5.54		
	333	−5.13		
150	298	−5.57	−12.13	−22.01
	303	−5.46		
	313	−5.24		
	323	−5.02		
	333	−4.80		
200	298	−5.22	−7.793	−8.63
	303	−5.18		
	313	−5.09		
	323	−5.01		
	333	−4.92		

Fig. 10. Possible adsorption mechanism.

determines the force of the adsorption. At the same initial concentration of ORII, the value of ΔG^0 increased with the temperature increasing, suggesting that the degree of randomness decreased and the adsorption became less favorable at higher temperatures.

3.6. Possible adsorption mechanism

Fig. 10 illustrates the mechanism for the adsorption of ORII onto MCS-NH_2. Under acidic and neutral conditions, the amino groups on MCS-NH_2 protonated to the cationic form (NH_3^+) and exhibited a stronger electrostatic interaction with negatively charged anionic dye ORII, MCS-NH_2 showed effective at binding sulfonate groups when the solution was at pH 3–7, as shown in Fig. 5(e). In addition, the hydrogen bonding between the amino and hydroxyl in MCS-NH_2 and sulfonate groups in ORII was also involved in the adsorption [55]. At alkaline conditions, more OH^- competed with the anionic ORII molecules on the surface of MCS-NH_2 while OH^- predominated [44], thus ORII removal decreased. Meanwhile, the reversible heterogeneous surfaces of MCS-NH_2 and the exothermic, decreased randomness, and spontaneous nature of adsorption process indicated the complex adsorption interactions of ORII adsorption onto MCS-NH_2 composite.

4. Conclusions

In this study, magnetic Fe_3O_4 coated with amino-functionalized magnetic chitosan composite was synthesized simply by one-pot method. The feasibility of MCS-NH_2 composite for the removal of anionic dye ORII from an aqueous solution was investigated systematically. The adsorbent exhibited excellent adsorption properties toward ORII due to the introduction of amino and hydroxyl groups. The pseudo-second-order equation better described the adsorption ORII as evidenced from the better correlation coefficient values as well as better-predicted value for $q_{e,exp}$. Freundlich isotherm model gave better correlation with the experimental data suggested reversible heterogeneous surfaces of MCS-NH_2. The thermodynamic analysis shows the spontaneous and exothermic nature of ORII adsorption onto MCS-NH_2 composite. Desorption and regeneration studies indicated that the adsorbent can be reused efficiently for three cycles. Based on its excellent adsorption performance, it can be concluded that MCS-NH_2 could be used as a low-cost and efficient adsorbent for removal of anionic dye from wastewater.

References

[1] N.M. Mahmoodi, Z. Mokhtari-Shourijeh, Preparation of PVA-chitosan blend nanofiber and its dye removal ability from colored wastewater, Fibers Polym., 16 (2015) 1861–1869.
[2] E. Pajootan, M. Arami, N.M. Mahmoodi, Binary system dye removal by electrocoagulation from synthetic and real colored wastewaters, J. Taiwan Inst. Chem. Eng., 43 (2012) 282–290.
[3] A. Abdolali, W.S. Guo, H.H. Ngo, S.S. Chen, N.C. Nguyen, K.L. Tung, Typical lignocellulosic wastes and by-products for biosorption process in water and wastewater treatment: a critical review, Bioresour. Technol., 160 (2014) 57–66.
[4] D.K. Patel, D.R. Tipre, S.R. Dave, Enzyme mediated bacterial biotransformation and reduction in toxicity of 1:2 chromium complex AB193 and AB194 dyes, J. Taiwan Inst. Chem. Eng., 77 (2017) 1–9.
[5] M.T. Yagub, T.K. Sen, S. Afroze, H.M. Ang, Dye and its removal from aqueous solution by adsorption: a review, Adv. Colloid Interface Sci., 209 (2014) 172–184.
[6] A. Dalvand, R. Nabizadeh, M.R. Ganjali, M. Khoobi, S. Nazmara, A.H. Mahvi, Modeling of Reactive Blue 19 azo dye removal from colored textile wastewater using L-arginine-functionalized Fe_3O_4 nanoparticles: optimization, reusability, kinetic and equilibrium studies, J. Magn. Magn. Mater., 404 (2016) 179–189.
[7] Y.R. Zhang, S.L. Shen, S.Q. Wang, J. Huang, P. Su, Q.R. Wang, B.X. Zhao, A dual function magnetic nanomaterial modified with lysine for removal of organic dyes from water solution, Chem. Eng. J., 239 (2014) 250–256.
[8] A.A. Atia, A.M. Donia, W.A. Al-Amrani, Adsorption/desorption behavior of acid orange 10 on magnetic silica modified with amine groups, Chem. Eng. J., 150 (2009) 55–62.
[9] S. Shariati, M. Faraji, Y. Yamini, A.A. Rajabi, Fe_3O_4, magnetic nanoparticles modified with sodium dodecyl sulfate for removal of safranin O dye from aqueous solutions, Desalination, 270 (2011) 160–165.
[10] Z. Chen, J. Wang, Z. Pu, Y. Zhao, D. Jia, H. Chen, T. Wen, B. Hu, A. Alsaedi, T. Hayat, X. Wang, Synthesis of magnetic Fe_3O_4/CFA composites for the efficient removal of U(VI) from wastewater, Chem. Eng. J., 320 (2017) 448–457.
[11] N. Limchoowong, P. Sricharoen, Y. Areerob, P. Nuengmatcha, T. Sripakdee, S. Techawongstien, S. Chanthai, Preconcentration and trace determination of copper (II) in Thai food recipes using Fe_3O_4@Chi–GQDs nanocomposites as a new magnetic adsorbent, Food Chem., 230 (2017) 388–397.
[12] M. Martínez-Quiroz, E.A. López-Maldonado, A. Ochoa-Terán, G.E. Pina-Luis, M.T. Oropeza-Guzman, Modification of chitosan with carbamoyl benzoic acids for testing its coagulant-flocculant and binding capacities in removal of metallic ions typically contained in plating wastewater, Chem. Eng. J., 332 (2018) 749–756.
[13] J.B. Marroquin, K.Y. Rhee, S.J. Park, Chitosan nanocomposite films: enhanced electrical conductivity, thermal stability, and mechanical properties, Carbohydr. Polym., 92 (2013) 1783–1791.
[14] S.A. Çetinus, E. Şahin, D. Saraydin, Preparation of Cu(II) adsorbed chitosan beads for catalase immobilization, Food Chem., 114 (2009) 962–969.
[15] S. Olivera, H.B. Muralidhara, K. Venkatesh, V.K. Guna, K. Gopalakrishna, Y. Kumar K., Potential applications of cellulose and chitosan nanoparticles/composites in wastewater treatment: a review, Carbohydr. Polym., 153 (2016) 600–618.
[16] P. Kanmani, J. Aravind, M. Kamaraj, P. Sureshbabu, S. Karthikeyan, Environmental applications of chitosan and cellulosic biopolymers: a comprehensive outlook, Bioresour. Technol., 242 (2017) 295–303.

[17] F. Zhao, B. Yu, Z. Yue, T. Wang, X. Wen, Z. Liu, C. Zhao, Preparation of porous chitosan gel beads for copper(II) ion adsorption, J. Hazard. Mater., 147 (2007) 67–73.
[18] Z. Rahimi, A.A. Zinatizadeh, S. Zinadini, Milk processing wastewater treatment in a bioreactor followed by an antifouling O-carboxymethyl chitosan modified Fe_3O_4/PVDF ultrafiltration membrane, J. Ind. Eng. Chem., 38 (2016) 103–112.
[19] Y. Luo, Z. Zhou, T. Yue, Synthesis and characterization of nontoxic chitosan-coated Fe_3O_4 particles for patulin adsorption in a juice-pH simulation aqueous, Food Chem., 221 (2017) 317–323.
[20] T. Li, Y. Liu, Q. Peng, X. Hu, T. Liao, H. Wang, M. Lu, Removal of lead(II) from aqueous solution with ethylenediamine-modified yeast biomass coated with magnetic chitosan microparticles: kinetic and equilibrium modeling, Chem. Eng. J., 214 (2013) 189–197.
[21] H.V. Tran, L.D. Tran, T.N. Nguyen, Preparation of chitosan/magnetite composite beads and their application for removal of Pb(II) and Ni(II) from aqueous solution, Mater. Sci. Eng., C, 30 (2010) 304–310.
[22] S.K. Kazy, S.K. Das, P. Sar, Lanthanum biosorption by a *Pseudomonas* sp.: equilibrium studies and chemical characterization, J. Ind. Microbiol. Biotechnol., 33 (2006) 773–783.
[23] L. Zhou, Z. Liu, J. Liu, Q. Huang, Adsorption of Hg(II) from aqueous solution by ethylenediamine-modified magnetic cross-linking chitosan microspheres, Desalination, 258 (2010) 41–47.
[24] G.Y. Li, K.L. Huang, Y.R. Jiang, D.L. Yang, P. Ding, Preparation and characterization of *Saccharomyces cerevisiae* alcohol dehydrogenase immobilized on magnetic nanoparticles, Int. J. Biol. Macromol., 42 (2008) 405–412.
[25] M. Gao, D. Zhang, W. Li, J. Chang, Q. Lin, D. Xu, H. Ma, Degradation of methylene blue in a heterogeneous Fenton reaction catalyzed by chitosan crosslinked ferrous complex, J. Taiwan Inst. Chem. Eng., 67 (2016) 355–361.
[26] L. Zhou, J. Xu, X. Liang, Z. Liu, Adsorption of platinum (IV) and palladium (II) from aqueous solution by magnetic cross-linking chitosan nanoparticles modified with ethylenediamine, J. Hazard. Mater., 182 (2010) 518–524.
[27] X. Sun, L. Yang, Q. Li, J. Zhao, X. Li, X. Wang, H. Liu, Amino-functionalized magnetic cellulose nanocomposite as adsorbent for removal of Cr(VI): synthesis and adsorption studies, Chem. Eng. J., 241 (2014) 175–183.
[28] N.A. Abdelwahab, F.M. Helaly, Simulated visible light photo-catalytic degradation of Congo red by TiO_2 coated magnetic polyacrylamide grafted carboxymethylated chitosan, J. Ind. Eng. Chem., 50 (2017) 162–171.
[29] B.C. Kholkhoev, S.A. Bal'Zhinov, V.G. Makotchenko, V.E. Fedorov, I.A. Farion, M.N. Kozlova, P.S. Timashev, V.F. Burdukovskii, Convenient approach to making nanocomposites based on a chitosan–poly (vinyl pyrrolidone) polymer matrix and a graphene nanofiller, J. Appl. Polym. Sci., 134 (2017) 45038.
[30] W. Liu, Q. Yang, Z. Yang, W. Wang, Adsorption of 2, 4-D on magnetic graphene and mechanism study, Colloids Surf., A, 509 (2016) 367–375.
[31] T.S. Anirudhan, S. Rijith, A.R. Tharun, Adsorptive removal of thorium(IV) from aqueous solutions using poly(methacrylic acid)-grafted chitosan/bentonite composite matrix: process design and equilibrium studies, Colloids Surf., A, 368 (2010) 13–22.
[32] R. He, X. You, J. Shao, F. Gao, B. Pan, D. Cui, Core/shell fluorescent magnetic silica-coated composite nanoparticles for bioconjugation, Nanotechnology, 18 (2017) 315601–315607.
[33] S. Srivastava, S.B. Agrawal, M.K. Mondal, Synthesis, characterization and application of *Lagerstroemia speciosa* embedded magnetic nanoparticle for Cr (VI) adsorption from aqueous solution, J. Environ. Sci., 55 (2017) 283–293.
[34] D. Zhao, G. Sheng, J. Hu, C. Chen, X. Wang, The adsorption of Pb(II) on Mg_2Al layered double hydroxide, Chem. Eng. J., 171 (2011) 167–174.
[35] J. Zhang, L. Li, Y. Li, C. Yang, Microwave-assisted synthesis of hierarchical mesoporous nano-TiO_2/cellulose composites for rapid adsorption of Pb^{2+}, Chem. Eng. J., 313 (2017) 1132–1141.
[36] S. Pandey, S.B. Mishra, Organic-inorganic hybrid of chitosan/organoclay bionanocomposites for hexavalent chromium uptake, J. Colloid Interface Sci., 361 (2011) 509–520.
[37] X.Y. Huang, J.P. Bin, H.T. Bu, G.B. Jiang, M.H. Zeng, Removal of anionic dye eosin Y from aqueous solution using ethylenediamine modified chitosan, Carbohydr. Polym., 84 (2011) 1350–1356.
[38] V.N. Tirtom, A. Dinçer, S. Becerik, T. Aydemir, A. Çelik, Comparative adsorption of Ni(II) and Cd(II) ions on epichlorohydrin crosslinked chitosan–clay composite beads in aqueous solution, Chem. Eng. J., 197 (2012) 379–386.
[39] G.Z. Kyzas, N.K. Lazaridis, Reactive and basic dyes removal by sorption onto chitosan derivatives, J. Colloid Interface Sci., 331 (2009) 32–39.
[40] Y.A. Aydın, N.D. Aksoy, Adsorption of chromium on chitosan: optimization, kinetics and thermodynamics, Chem. Eng. J., 151 (2009) 188–194.
[41] W. Konicki, M. Aleksandrzak, D. Moszyński, E. Mijowska, Adsorption of anionic azo-dyes from aqueous solutions onto graphene oxide: equilibrium, kinetic and thermodynamic studies, J. Colloid Interface Sci., 496 (2017) 188–200.
[42] L. Zhou, J. Jin, Z. Liu, X. Liang, C. Shang, Adsorption of acid dyes from aqueous solutions by the ethylenediamine-modified magnetic chitosan nanoparticles, J. Hazard. Mater., 185 (2011) 1045–1052.
[43] L. Obeid, A. Bée, D. Talbot, S.B. Jaafar, V. Dupuis, S. Abramson, V. Cabuil, M. Welschbillig, Chitosan/maghemite composite: a magsorbent for the adsorption of methyl orange, J. Colloid Interface Sci., 410 (2013) 52–58.
[44] X. Hu, J. Wang, Y. Liu, X. Li, G. Zeng, Z. Bao, X. Zeng, A. Chen, F. Long, Adsorption of chromium (VI) by ethylenediamine-modified cross-linked magnetic chitosan resin: isotherms, kinetics and thermodynamics, J. Hazard. Mater., 185 (2011) 306–314.
[45] K. Vijayalakshmi, B.M. Devi, S. Latha, T. Gomathi, P.N. Sudha, J. Venkatesan, S. Anil, Batch adsorption and desorption studies on the removal of lead (II) from aqueous solution using nanochitosan/sodium alginate/microcrystalline cellulose beads, Int. J. Biol. Macromol., 104 (2017) 1483–1494.
[46] C. Lin, S. Li, M. Chen, R. Jiang, Removal of Congo red dye by gemini surfactant C_{12}-4-C_{12}·2Br-modified chitosan hydrogel beads, J. Dispersion Sci. Technol., 38 (2016) 46–57.
[47] Y. Hu, T. Guo, X. Ye, Q. Li, M. Guo, H. Liu, Z. Wu, Dye adsorption by resins: effect of ionic strength on hydrophobic and electrostatic interactions, Chem. Eng. J., 228 (2013) 392–397.
[48] J. Wang, H. Zhu, C. Hurren, J. Zhao, E. Pakdel, Z. Li, X. Wang, Degradation of organic dyes by P_{25}-reduced graphene oxide: influence of inorganic salts and surfactants, J. Environ. Chem. Eng., 3 (2015) 1437–1443.
[49] B.C. Pires, F.V.A. Dutra, T.A. Nascimento, K.B. Borges, Preparation of PPy/cellulose fibre as an effective potassium diclofenac adsorbent, React. Funct. Polym., 113 (2017) 40–49.
[50] C. Liu, R.N. Jin, X.K. Ouyang, Y.G. Wang, Adsorption behavior of carboxylated cellulose nanocrystal—polyethyleneimine composite for removal of Cr(VI) ions, Appl. Surf. Sci., 408 (2017) 77–87.
[51] M.O. Ansari, R. Kumar, S.A. Ansari, S.P. Ansari, M.A. Barakat, A. Alshahrie, M.H. Cho, Anion selective pTSA doped polyaniline@ graphene oxide-multiwalled carbon nanotube composite for Cr(VI) and Congo red adsorption, J. Colloid Interface Sci., 496 (2017) 407–415.
[52] S. Hokkanen, A. Bhatnagar, A. Koistinen, T. Kangas, U. Lassi, M. Sillanpää, Comparison of adsorption equilibrium models and error functions for the study of sulfate removal by calcium hydroxyapatite microfibrillated cellulose composite, Environ. Technol., 39 (2018) 952–966.
[53] R. Ahmad, I. Hasan, L-cystein modified bentonite-cellulose nanocomposite (cellu/cys-bent) for adsorption of Cu^{2+}, Pb^{2+}, and Cd^{2+} ions from aqueous solution, Sep. Sci. Technol., 51 (2016) 381–394.
[54] C. Ding, Y. Sun, Y. Wang, J. Li, Y. Lin, W. Sun, C. Luo, Adsorbent for resorcinol removal based on cellulose functionalized with magnetic poly(dopamine), Int. J. Biol. Macromol., 99 (2017) 578–585.
[55] E. Salehi, P. Daraei, A.A. Shamsabadi, A review on chitosan-based adsorptive membranes, Carbohydr. Polym., 152 (2016) 419–432.